

Learning about the Recent Star Formation History of Galaxy Disks by Comparing their Far-Infrared and Radio Morphologies: Cosmic-Ray Electron Diffusion after Star Formation Episodes

E.J. Murphy,¹ G. Helou,² J.D.P. Kenney,¹ L. Armus,³ and R. Braun⁴

ABSTRACT

We present results on the interstellar medium (ISM) properties of 29 galaxies based on a comparison of *Spitzer* far-infrared and Westerbork Synthesis Radio Telescope radio continuum imagery. Of these 29 galaxies, 18 are close enough to resolve at $\lesssim 1$ kpc scales at $70\ \mu\text{m}$ and $22\ \text{cm}$. We extend the Murphy et al. (2006a,b) approach of smoothing infrared images to approximate cosmic-ray (CR) electron spreading and thus largely reproduce the appearance of radio images.

Using a wavelet analysis we decompose each $70\ \mu\text{m}$ image into one component containing the star-forming *structures* and a second one for the diffuse *disk*. The components are smoothed separately, and their combination compared to a free-free corrected $22\ \text{cm}$ radio image; the scale-lengths are then varied to best match the radio and smoothed infrared images. We find that late-type spirals having high amounts of ongoing star formation benefit most from the two-component method. We also find that the disk component dominates for galaxies having low star formation activity, whereas the structure component dominates at high star formation activity.

We propose that this result arises from an age effect rather than from differences in CR electron diffusion due to varying ISM parameters. The bulk of the CR electron population in actively star-forming galaxies is significantly younger than that in less active galaxies due to recent episodes of enhanced star formation; these galaxies are observed within $\sim 10^8$ yr since the onset of the most recent star formation episode. The sample irregulars have anomalously low best-fit scale-lengths for their surface brightnesses compared to the rest of the sample spirals which we attribute to enhanced CR electron escape.

Subject headings: galaxies: ISM — infrared: galaxies — infrared: ISM — radio continuum: galaxies — cosmic-rays

1. Introduction

To date, most of our knowledge about the relativistic phase of the interstellar medium (ISM) outside of the Galaxy, consisting of relativistic charged particles and magnetic fields, has been obtained indirectly through the detection of synchrotron emission via multi-frequency radio observations (e.g. Duric 1991;

¹Department of Astronomy, Yale University, P.O. Box 208101, New Haven, CT 06520-8101; murphy@astro.yale.edu

²California Institute of Technology, MC 314-6, Pasadena, CA 91125

³*Spitzer* Science Center, California Institute of Technology, Pasadena, CA 91125

⁴ASTRON, P.O. Box 2, 7990 AA Dwingeloo, The Netherlands

Dahlem, Lisenfeld, & Golla 1995; Lisenfeld et al. 1996; Irwin et al. 1999; Beck 2005). Synchrotron emission arises from cosmic-ray (CR) electron energy losses as these particles are accelerated in the magnetic fields of galaxies. Although the energy density in CR electrons is only $\sim 1\%$ of that for CR nuclei, the similarity between the spatial distributions of gamma-ray and synchrotron emission within the Galaxy suggests that CR electrons and CR nuclei are fairly well mixed on the scales of a few hundred parsecs (e.g. Haslam et al. 1982; Bloemen et al. 1986; Webber 1991). The spatial distribution of a galaxy’s synchrotron emission is a function of a galaxy’s CR electron and magnetic field distributions. Thus, radio synchrotron maps provide only limited insight on the source distribution of the CR electrons as well as the distances the particles may have traveled before ending up in their current location of emission.

Massive stars ($\gtrsim 8 M_{\odot}$) are the progenitors of supernovae (SNe) whose remnants (SNRs), through the process of diffusive shock acceleration (Bell 1978; Blandford & Ostriker 1978), appear to be the main acceleration sites of CR electrons responsible for a galaxy’s observed synchrotron emission. These same young massive stars are often the primary sources for dust heating as they emit photons which are re-radiated at far-infrared (FIR) wavelengths. This shared origin between the FIR and radio emission of galaxies is thought to be the foundation for the observed FIR-radio correlation among (e.g. de Jong et al. 1985; Helou, Soifer, & Rowan-Robinson 1985; Niklas 1997; Niklas & Beck 1997; Yun, Reddy, & Condon 2001) and within galaxies (e.g. Beck & Golla 1988; Xu et al. 1992; Marsh & Helou 1995; Hoernes, Berkhuijsen, & Xu 1998; Hippelein et al. 2003; Murphy et al. 2006a; Hughes et al. 2006).

Coupling the shared origin of a galaxy’s FIR and radio emission with the fact that the mean free path of dust-heating photons (~ 100 pc) is significantly shorter than the expected diffusion length of CR electrons (~ 1 -2 kpc) led Bica & Helou (1990) to conjecture that the radio image of a galaxy should resemble a smoothed version of its infrared image. Consequently, it appears that the close spatial correlation between the FIR and radio continuum emission within galaxies can be used to characterize the propagation history of CR electrons. This prescription has been shown to hold for galaxies observed at the “super resolution” ($\lesssim 1'$) of *IRAS* HIREs data (Marsh & Helou 1998) and, more recently, for high resolution ($\sim 18''$) *Spitzer* 70 μm imaging (Murphy et al. 2006a, hereafter M06a). This phenomenology has been further corroborated on scales $\gtrsim 50$ pc by Hughes et al. (2006) who find synchrotron haloes around individual star-forming regions are more extended than FIR-emitting regions within the Large Magellanic Cloud.

Murphy et al. (2006b, hereafter, M06b) recently studied how the spatial distributions of a galaxy’s FIR and radio emission vary as a function of the intensity of star formation. They concluded that CR electrons are, on average, younger and closer to their place of origin within galaxies having higher amounts of star formation activity compared with more quiescent galaxies. Using a wavelet-based image decomposition, we extend this work by attempting to characterize separately CR electron populations associated with a galaxy’s diffuse disk and its star-forming complexes. We carry out this study for a sample of galaxies observed as part of the *Spitzer* Infrared Nearby Galaxies Survey (SINGS; Kennicutt et al. 2003) and the Westerbork Synthesis Radio Telescope (WSRT-SINGS; Braun et al. 2007) for which we have the spatial resolution to resolve physical scales < 1 kpc. The complete study can be found in Murphy et al. (2008).

2. Observations and Analysis

Observations at 24, 70, and 160 μm were obtained using the Multiband Imaging Photometer for *Spitzer* (MIPS; Rieke, et al. 2004) as part of the SINGS legacy science program. A detailed description of the SINGS observational strategy can be found in Kennicutt et al. (2003). Radio continuum imaging at 22 cm

was performed using the Westerbork Synthesis Radio Telescope (WSRT) as part of the WSRT-SINGS survey. A complete description of the radio observations and image processing steps can be found in Braun et al. (2007). We match the resolution of the MIPS and radio images using Gaussian PSFs rather than the MIPS PSFs, which suffer from significant power in their side-lobes.

We compute the radiation field energy density (U_{rad}) of each galaxy using its TIR ($3 - 1100 \mu\text{m}$) surface brightness since this parameter is sensitive to the diffusion of CR electrons. Using the deprojected area of elliptical apertures (A_{TIR}), we calculate TIR surface brightnesses ($\Sigma_{\text{TIR}} = L_{\text{TIR}}/A_{\text{TIR}}$) along with estimates of U_{rad} for radiation emitted near the surface of a semi-transparent body such that

$$U_{\text{rad}} \approx \frac{2\pi}{c} I_{\text{bol}} \gtrsim \frac{L_{\text{TIR}}}{2A_{\text{TIR}}c} \left(1 + \sqrt{\frac{3.8 \times 10^{42}}{L_{\text{TIR}}}} \right), \quad (1)$$

where I_{bol} is a galaxy’s bolometric surface brightness, c is the speed of light, and all quantities are given in cgs units. The parenthetical term in Equation 1 provides a correction for non-absorbed UV emission that was empirically derived by Bell (2003) using archived FIR and UV data for a sample of more than 200 galaxies.

2.1. Multi-Component Image-Smearing Model

Using a phenomenological image-smearing model, first presented by Bica & Helou (1990), M06b studied how the spatial distributions of FIR and radio emission varied as a function of star-formation intensity within 12 spiral galaxy disks. The basic procedure used here is similar to that presented in M06a,b. We calculate and minimize the residuals between the free-free corrected radio and observed infrared images after convolving the infrared maps by a parameterized kernel $\kappa(\mathbf{r})$. The new element is that we now, using a wavelet-based technique, decompose each observed infrared image, into two sub-images: (1) a *structure* image containing features with spatial scale smaller than 1 kpc; (2) a *disk* image containing all structures with characteristic spatial scales larger than or equal to 1 kpc, largely constituting a galaxy’s diffuse disk. The *structure* and *disk* images are smeared independently, summed, and then compared to the radio image. For a full description of the phenomenological model we refer the reader to Murphy et al. (2008).

3. Discussion

By plotting the smearing scale-length which best matches the infrared image to the observed radio map versus TIR surface brightness (see Figure 1), we find that the FIR and non-thermal radio morphologies are more similar to each other for galaxies having higher radiation field energy densities compared to galaxies with lower radiation field energy densities. Following the interpretation of M06b, our results indicate that CR electrons are, on average, closer to their place of origin in galaxies having higher star formation activity.

As CR electrons propagate through the ISM of galaxies they lose their energy due to a number physical processes including synchrotron, inverse-Compton (IC) scattering, bremsstrahlung, ionization, and adiabatic expansion losses. In normal galaxies synchrotron and IC scattering processes are likely the most significant energy loss terms for CR electrons associated with 1 GHz emission (Condon 1992); the other terms listed will become non-negligible, however, for galaxies hosting extreme episodes of star-formation like starbursting ultra-luminous infrared galaxies (ULIRGs) (e.g. Thompson et al. 2006).

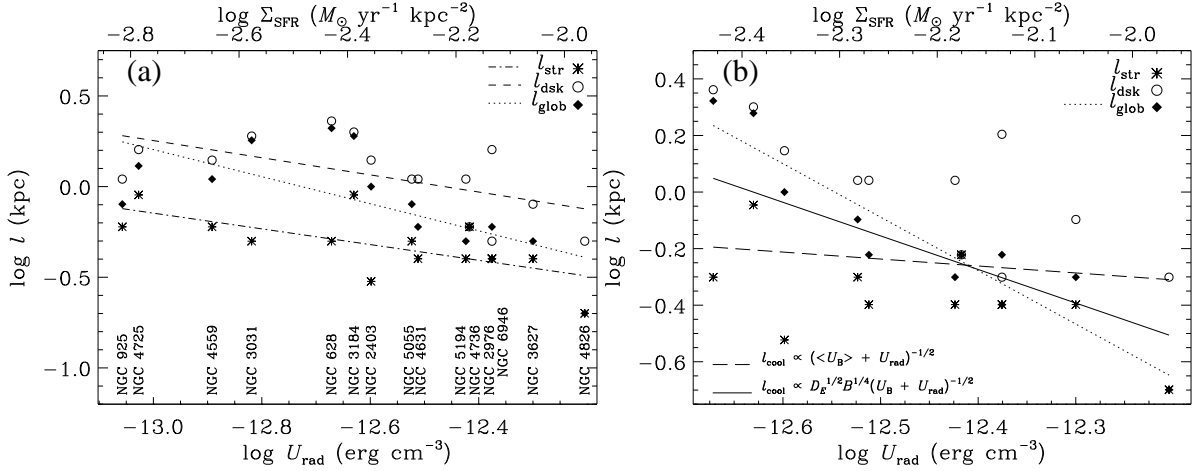


Fig. 1.— In panel (a) we plot the best-fit disk, structure, and global scale-lengths for galaxies in our sample which are resolved at scales less than 1 kpc against the radiation field energy densities, U_{rad} . We exclude the galaxies Holmb II, IC 2574, and NGC 4236 which have morphologies not well fit by our phenomenological model. Least square fits for the best-fit disk, structure, and global scale-lengths are plotted as *dot-dash*, *dashed*, and *dotted lines*, respectively. In panel (b) we have excluded the galaxies NGC 925, NGC 4725, NGC 4559, and NGC 3031 due to possible signal-to-noise effects. Along with the fit to the global scale-lengths (*dotted line*) we also plot with the expected diffusion scale-lengths due to inverse Compton (IC) losses in a fixed magnetic field (*long-dashed line*) and synchrotron + IC losses with an energy-dependent diffusion coefficient D_E for the steepest possible index (*solid line*). The slope of our observed trend is clearly steeper than what is achieved by our scaling-relations; this suggests that the variation of ISM parameters alone cannot explain out observations.

A CR electron having energy E will emit most of its energy at a critical frequency ν_c where

$$\left(\frac{\nu_c}{\text{GHz}}\right) = 1.3 \times 10^{-2} \left(\frac{B}{\mu\text{G}}\right) \left(\frac{E}{\text{GeV}}\right)^2. \quad (2)$$

From this, we can express the effective cooling timescale for CR electrons due to synchrotron and IC losses as

$$\left(\frac{\tau_{\text{cool}}}{\text{yr}}\right) \sim 5.7 \times 10^7 \left(\frac{\nu_c}{\text{GHz}}\right)^{-1/2} \left(\frac{B}{\mu\text{G}}\right)^{1/2} \left(\frac{U_B + U_{\text{rad}}}{10^{-12} \text{ erg cm}^{-3}}\right)^{-1}. \quad (3)$$

In simple diffusion models, the propagation of CR electrons is usually characterized by an empirical, energy-dependent diffusion coefficient, D_E (e.g. Ginzburg et al. 1980). The value of D_E has been found to be around $4 - 6 \times 10^{28} \text{ cm}^2 \text{ s}^{-1}$ for $\lesssim \text{GeV}$ CRs by fitting diffusion models with direct measurements of CR nuclei (i.e. secondary-to-primary ratios like Boron-to-Carbon) within the Solar Neighborhood (e.g. Moskalenko et al. 2002). We will assume,

$$\left(\frac{D_E}{\text{cm}^2 \text{ s}^{-1}}\right) \sim \begin{cases} 5 \times 10^{28}, & E < 1 \text{ GeV} \\ 5 \times 10^{28} \left(\frac{E}{\text{GeV}}\right)^{1/2}, & E \geq 1 \text{ GeV}. \end{cases} \quad (4)$$

Now, neglecting escape and using a simple random-walk equation, CR electrons will diffuse a distance $l_{\text{cool}} = (D_E \tau_{\text{cool}})^{1/2}$ before losing all of their energy to synchrotron and IC losses. By combining Equations 2 and 4, we can express D_E as a function of B for a fixed ν_c such that, for CR electrons having energies $\geq 1 \text{ GeV}$,

$$\left(\frac{l_{\text{cool}}}{\text{kpc}}\right) \sim 7 \times 10^{-4} \left(\frac{\tau_{\text{cool}}}{\text{yr}}\right)^{1/2} \left(\frac{\nu_c}{\text{GHz}}\right)^{1/8} \left(\frac{B}{\mu\text{G}}\right)^{-1/8}. \quad (5)$$

3.1. Order of Magnitude Estimates

Using the above equations, we derive simple, order-of-magnitude estimates to determine whether diffusion and cooling of CR electrons in a steady-state star formation model are able to account for our observations. Taking the mean value of U_{rad} for those galaxies plotted in Figure 1b (i.e. $3.7 \times 10^{-13} \text{erg cm}^{-3}$), and assuming $U_{\text{rad}} = U_{\text{B}}$, which has been shown to be a reasonable assumption for a large sample of spiral galaxies (Lisenfeld, Völk, & Xu 1996), we find from Equation 3 that the average cooling time for a 1.4 GHz emitting CR electron is $\sim 1.1 \times 10^8$ yr. Inserting this value into Equation 5, we measure a diffusion scale-length of ~ 6.8 kpc; this value is clearly off of the scale shown in Figure 1b. On the other hand, if we instead assume a fixed, typical magnetic field strength of $9 \mu\text{G}$ (Niklas 1995), and that $U_{\text{B}} = U_{\text{rad}} = 3.2 \times 10^{-12} \text{erg cm}^{-3}$, the average cooling time for a 1.4 GHz emitting CR electron is $\sim 2.2 \times 10^7$ yr with a diffusion scale-length of ~ 2.6 kpc. While this value for U_{rad} is much higher than what we infer from the average TIR surface brightness of the sample, it must apply near bright star-forming structures, whose TIR surface brightnesses are much greater. Even so, this diffusion scale-length is much larger than any value we find for the best-fit structure scale-lengths. From these simple order of magnitude estimates it appears that particle fading due to cooling by Inverse Compton and synchrotron processes alone cannot explain the structural differences between the FIR and radio maps; the best explanation seems to be differences in the CR electron population ages.

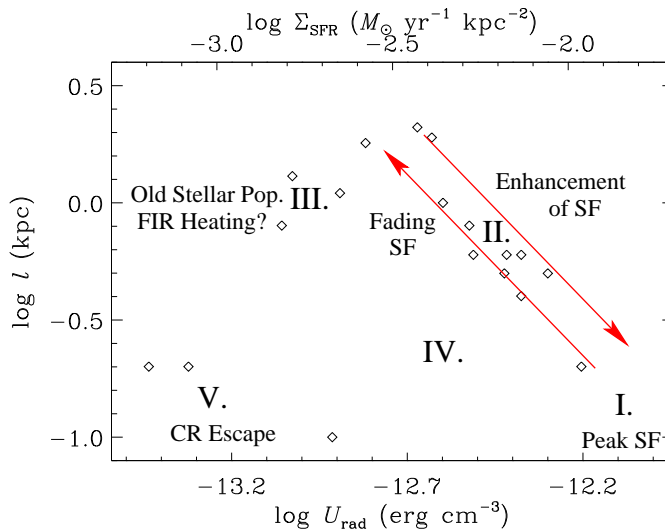


Fig. 2.— The best-fit global scale-lengths for the entire 18 galaxy sample using isotropic kernels having an exponential profile and our free-free corrected radio maps. Overplotted on the scatter diagram are roman numerals to identify the general placement of galaxies on this diagram; these locations are discussed in the text.

3.2. Morphologies of Star Formation

In order to provide a physical interpretation for the location of galaxies in the best-fit scale-length— U_{rad} diagram, we describe their general locations, designated by roman numerals, in Figure 2. While the placement of NGC 925, NGC 4725, NGC 4559 in Figure 1a may be the result of a signal-to-noise effect, we will now consider alternative physical explanations. The irregular galaxies in our sample (Holmb II, IC 2574, and NGC 4236) have also been excluded thus far in our discussion due to their lack of a disk component in

the FIR and radio. The placement of these objects in Figure 2 and their behavior will now be put into the context of our phenomenological picture.

- I. In this region of the diagram we assume a galaxy has just reached a peak in its surface brightness after a recent episode of enhanced star formation; the episode must have occurred within the last few Myr to ensure that SNRs are still relatively young and that the morphologies of the radio and infrared emission are similar because CR electrons have not had time to diffuse very far.
- II. After reaching a peak in global star formation activity, those CR electrons associated with the recent enhancement of star formation will dominate the CR population. As they spread through the galaxy they will begin to lose their energy to synchrotron and IC processes. A galaxy’s position along this trend cannot be due to variations in ISM parameters alone; rather, its star formation history is the dominant parameter (see Figure 1b). Galaxies may move along this part of phase space as star formation activity becomes enhanced and then fades.
- III. Galaxies in this region are characterized by low star formation activity and have best-fit scale-lengths which are shorter than expected given the trend found in region II. While this situation can be explained by a signal-to-noise effect, it can also be explained by a significant amount of FIR emission arising from an old stellar population.
- IV. We find no galaxies occupying this region of phase space in which relatively short global scale-lengths would be measured for a moderate values of U_{rad} . One way for a galaxy to populate this part of the diagram is if, after a long period of quiescence, it begins to form stars at a moderate rate. The galaxy would then pass through this region very quickly ($\lesssim 10^7$ yr) before shifting into region II. The lack of such galaxies suggests that, at least in the local Universe, star formation in spirals does not completely cease for long periods of time.
- V. The irregulars behave markedly different than the sample spirals. We do not believe this discrepant behavior to be the result of signal-to-noise effects. The morphologies and ISM of these galaxies do not seem consistent with keeping their CR electrons bound outside of their initial clouds around SNRs. After the CR electrons leave this cloud, the lack of a dense ISM and magnetic field to keep them trapped through multiple scatterings off of magneto-hydrodynamic (MHD) waves allows them to easily escape the system and enter intergalactic space.

4. Summary and Conclusions

Using a two-component image-smearing analysis, we have separated the signatures of CR electron diffusion at spatial scales corresponding to star-forming structures (< 1 kpc) and galaxy disks (≥ 1 kpc) within 18 galaxies observed as part of SINGS and WSRT-SINGS. Our results and conclusions can be summarized as follows:

1. The best-fit global scale-lengths decrease as a function of increasing star formation activity as measured by the infrared surface brightness of a galaxy. Our interpretation is that a galaxy’s CR electrons are closer to their place of origin within galaxies having intense star formation activity.
2. The trend of decreasing best-fit *global* scale-length with increasing radiation field energy density is due to higher surface brightness galaxies having undergone a recent enhancement of star formation

rather than variations in other ISM parameters. For sufficiently large enhancements, these galaxies are observed within $\sim 10^8$ yr of the onset of the most recent star formation episode.

3. Unlike spirals, irregular galaxies lack any well defined diffuse disk component at either $70 \mu\text{m}$, or especially at 22 cm. Presumably, the CR electrons escape these galaxies soon after leaving their parent star-forming regions due the absence of a dense ISM which would keep large-scale interstellar magnetic field locked into place. This conclusion helps to explain why these galaxies have global FIR/radio ratios systematically greater than canonical values.
4. As infrared surface brightness increases, the characteristic diffusion scale-length of a galaxy's CR electron population begins to transition at $\log U_{\text{rad}} \leq -12.5$ from being biased by CR electrons making up its diffuse disk to being biased by those recently injected near star-forming structures. From this we conclude that a galaxy's CR electron population transitions from being dominated by old CR electrons to being dominated by young CR electrons as a function of star formation intensity.
5. The two-component analysis works better than smearing with a single smoothing kernel for spiral galaxies of type Sb or later which have high amounts of ongoing star formation activity (i.e. $\sim 40\%$ of the sample). This result suggests that star formation must be intense and highly structured for the two-component analysis of these data to differentiate properly between the different CR electron populations.

E.J.M would also like to thank other members of the *Spitzer* Infrared Nearby Galaxies Survey (SINGS) team for their invaluable contributions to the work presented here, especially those of R.C.Kennicutt, Jr., D.Calzetti, K.D.Gordon, C.W.Engelbracht, and G.Bendo. As part of the *Spitzer* Space Telescope Legacy Science Program, support was provided by NASA through Contract Number 1224769 issued by the Jet Propulsion Laboratory, California Institute of Technology under NASA contract 1407.

REFERENCES

- Beck, R. 2005, in Cosmic Magnetic Fields, eds. R. Wielebinsky & R. Beck (Berlin: Springer), 41
- Beck, R. and Golla, G. 1988, A&A, 191, L9
- Bell, A. R. 1978, MNRAS, 182, 147
- Bell, E. F. 2003, ApJ, 586, 794
- Bicay M. D. and Helou, G. 1990, ApJ, 362, 59
- Blandford, R. D. and Ostriker, J. P. 1978, ApJ, 221, L29
- Bloemen, J. B. G. M., et al. 1986, A&A, 154, 25
- Braun, R., Oosterloo, T. A., Morganti, R., Klein, U., and Beck, R. 2007, A&A, 461, 455
- Condon, J. J. 1992, ARA&A, 30, 575
- Dahlem, M., Lisenfeld, U., and Golla, G. 1995, ApJ, 444, 119
- de Jong, T., Klein, U., Wielebinski, R., and Wunderlich, E. 1985, A&A, 147, L6

- Duric N. 1991, in ASP Conf. Ser. 18, The Interpretation of Modern Synthesis Observations of Spiral Galaxies, ed. N. Duric and P. Crane (San Francisco: ASP), 17
- Ginzburg, V. L., Khazan, Ya. M., and Ptuskin, V. S. 1980, *Ap&SS*, 68, 295
- Haslam, C. G. T., Stoffel, H., Salter, C. J., and Wilson, W. E. 1982, *A&AS*, 47, 1
- Helou, G., Soifer, B. T., and Rowan-Robinson, M. 1985, *ApJ*, 298, L7
- Hippelein, H., Haas, M., Tuffs, R. J., Lemke, D., Stickel, M., Klaas, U., and Völk, H. J. 2003, *A&A*, 407, 137
- Hoernes, P., Berkhuijsen, E. M., and Xu, C. 1998, *A&A*, 334, 57
- Hughes, A., Wong, T., Ekers, R., Staveley-Smith, L., Filipovic, M., Maddison, S., Fukui, Y., & Mizuno, N. 2006, *MNRAS*, 370, 363
- Irwin, J. A., English, J., and Sorathia, B. 1999, *AJ*, 117, 2102
- Kennicutt, R. C. Jr., et al. 2003, *PASP*, 115, 928
- Lisenfeld, U., Alexander, P., Pooley, G. G., and Wilding, T. 1996, *MNRAS*, 281, 301
- Lisenfeld, U., Völk, H. J., and Xu, C. 1996, *A&A*, 306, 677
- Marsh, K. A. and Helou, G. 1995, *ApJ*, 445, 599
- Marsh, K. A. and Helou, G. 1998, *ApJ*, 493, 121
- Moskalenko, I. V., Strong, A. W., Ormes, J. F., and Potgieter, M. S. 2002, *ApJ*, 565, 280
- Murphy E. J., et al. 2006, *ApJ*, 638, 157 (M06a)
- Murphy E. J., et al. 2006, *ApJ*, 651, L111 (M06b)
- Murphy, E.J., Helou, G., Kenney, J.D.P., Armus, L., and Braun, R. 2008, *ApJ*, 679, in press (arXiv:0801.4768)
- Niklas, S. 1995, Ph.D. thesis, Univ. Bonn
- Niklas, S. 1997, *A&A*, 322, 29
- Niklas, S. and Beck, R. 1997, *A&A*, 322, 54
- Rieke, G. H., et al. 2004, *ApJS*, 154, 25 *ApJ*, 493, 121
- Thompson, T. A., Quataert, E., Waxman, E., Murray, N., and Martin, C. L. 2006, *ApJ*, 645, 186
- Webber, W. R. 1991, in ASP Conf. Ser. 18, The Interpretation of Modern Synthesis Observations of Spiral Galaxies, ed. N. Duric and P. Crane (San Francisco: ASP), 27
- Xu, C., Klein, U., Meinert, D., Wielebinski, R., and Haynes, R. F. 1992, *A&A*, 257, 47
- Yun, M. S., Reddy, N. A., and Condon, J. J. 2001, *ApJ*, 554, 803